JACS
JOURNAL OF THE AMERICAN CHEMICAL SOCIETY
Article
Cite This: J. Am. Chem. Soc. XXXX, XXX, XXX−XXX
pubs.acs.org/JACS

Polarized Luminescence of Anisotropic $LaPO_4$:Eu Nanocrystal Polymorphs

Elodie Chaudan,[†] Jongwook Kim,*[,†] Sandrine Tusseau-Nenez,[†] Philippe Goldner,[‡] Oscar L. Malta,[§] Jacques Peretti,[†] and Thierry Gacoin*[,†]

[†]Laboratoire de Physique de la Matière Condensée, Ecole Polytechnique, CNRS, Université Paris-Saclay, 91128 Palaiseau, France
[‡]PSL Research University, Chimie ParisTech, CNRS, Institut de Recherche de Chimie Paris, 75005 Paris, France
[§]Department of Fundamental Chemistry, Federal University of Pernambuco, University City, CEP 50 Recife, Pernambuco, Brazil

Supporting Information

ABSTRACT: Lanthanide elements exhibit highly appealing spectroscopic properties that are extensively used for phosphor applications. Their luminescence contains precise information on the internal structure of the host materials. Especially, the polarization behavior of the transition sublevel peaks is a fingerprint of the crystal phase, symmetry, and defects. However, this unique feature is poorly explored in current research on lanthanide nanophosphors. We here report on a detailed investigation of the evolution of Eu^{3+} luminescence during the thermally induced phase transition of $LaPO_4$ nanocrystal hosts. By means of *c*-axis-aligned nanocrystal assemblies, we demonstrate a dramatic change of the emission polarization feature corresponding to the distinct Eu^{3+} site symmetries in different $LaPO_4$ polymorphs. We also show that changes of the nanocrystal structure can be identified by this spectroscopic method, with a much higher sensitivity than the X-ray diffraction analysis. This new insight into the nanostructure-luminescence relationship, associated with the unprecedented polarization characterizations, provides a new methodology to investigate phase transitions in nanomaterials. It also suggests a novel function of lanthanide emitters as orientation-sensing nanoprobes for innovative applications such as in bioimaging or microfluidics.

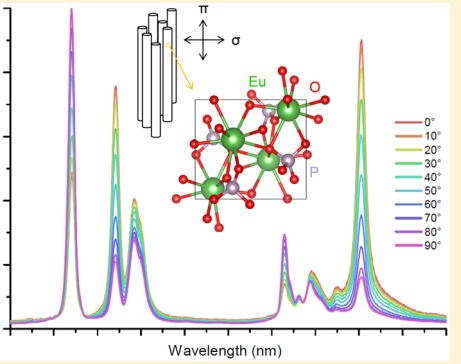

INTRODUCTION

Luminophores with anisotropic molecular or crystal structures or anisotropic morphology exhibit polarized emission properties.[1−5] This effect provides access to the fine structure and the spatial orientation of the emitting species.[6−8] Among them, semiconductor nanorods[2,3] are representative and modern examples showing a linear polarization behavior. However, their polarization behavior is not fully determined by the intrinsic properties of the material but depends on the size and shape of the particles.[9] Moreover, semiconductor particles usually exhibit a single emission band (at room temperature) with constant polarization across the line shape. These features limit the use of the polarized emission properties of semiconductor nanorods.

Meanwhile, the luminescence of lanthanide elements doped in anisotropic host materials manifests a polarization that is governed by the selection rules for their local site symmetries[10] and also by the crystal symmetry. In this case, crystal structures or coordination chemistries are the main parameters that influence luminescence polarization. Also, the multiple transition levels that are independently polarized result in a dramatic and informative variation of the spectral line shape.[11] Earlier studies using macroscopically grown single crystals with lanthanide dopants demonstrated that this phenomenon is useful for the identification of the crystal phase and defect states.[6−8] Nevertheless, in recent years, although a variety of lanthanide nanoparticle systems have been prepared particularly for nano- and bioprobe applications,[12,13] polarization phenomena have been almost neglected. This is presumably due to the random orientation of small particles in bulk states, such as colloidal solutions or powders resulting in unpolarized luminescence, and to the difficulty to measure the luminescence of a single particle with high signal-to-noise ratio.

Here, we report on a systematic study linking the structural properties of a nanocrystal with the luminescence and polarization characteristics of the lanthanide dopants. This is demonstrated by tracking the evolution of the polarized luminescence spectra driven by the thermally induced phase transformation of the nanocrystals. Our approach to avoid the problem of the random particle orientation is to align the main axes of the nanocrystals by means of self-assembly. In order to facilitate the crystal alignment with high degree of orientation, we synthesized monocrystalline lanthanum phosphate ($LaPO_4$) nanorods in hexagonal phase, the crystallographic *c*-axis of which is consistently parallel to the geometrical (long) axis.[14] As demonstrated previously, colloidal dispersions of these nanorods exhibit liquid crystalline self-assembly, and its

Received: April 17, 2018
Published: July 3, 2018

DOI: 10.1021/jacs.8b03983
J. Am. Chem. Soc. XXXX, XXX, XXX−XXX

orientation direction can be further controlled by applying a shear force.[15] This technique allows achieving finally a macroscopic monodomain, in which all nanocrystals are almost perfectly aligned. Once La^{3+} sites are partially substituted by other luminescent lanthanides such as Eu^{3+}, the monodomain samples exhibit photoluminescence as intense and well-polarized as a large single crystal.[15] We use such a nanorod-aligned monodomain sample, in which the *c*-axis direction is found to be conserved even along the complete phase transition from the hexagonal (rhabdophane) phase to the monoclinic (monazite) phase.[16,17]

Another way to investigate polarization phenomena of a nanoscale system is to perform spectroscopy at the single particle level. A few recent studies at the single particle level exist on the $NaYF_4$ doped with Tb^{3+}/Yb^{3+},[18] Er^{3+}/Yb^{3+},[19] and Er^{3+}.[20] These studies demonstrate the first examples of polarization dependence on the nanoparticle's orientation. However, such a single nanoparticle measurement requires sophisticated optical microscopies,[19] and the signal-to-noise ratio is often low. In contrast, our approach benefits from the nanocrystal alignment providing the luminescence intensity as large as from a macroscopic single crystal while enabling the investigation of the structure-luminescence relationship and its temperature-dependent evolution in nanoparticles, including the influence of the small size, the large surface, and the crystal growth under sintering. The continuous transition of the $LaPO_4$ nanocrystals from one to another polymorph by step annealing is tracked by both X-ray diffraction (XRD) and luminescence spectroscopy. Drastic changeovers in the photoluminescence spectrum were observed unexpectedly at intermediate temperatures where the phase transition of the macroscopic samples had not been observed. In addition, the polarization features of many single transition levels were precisely analyzed.

PREPARATION AND CHARACTERIZATION

$LaPO_4$:Eu nanorods, with 5% Eu doping, were hydrothermally synthesized and then dispersed in ethylene glycol by the following method. Aqueous solutions of $(NH_4)_2HPO_4$ (50 mM), $La(NO_3)_3 \times 6H_2O$ (47.5 mM) and $Eu(NO_3)_3 \times 5H_2O$ (2.5 mM) were mixed in a glass tube to precipitate seed particles. The tube was then sealed and heated in an oven at 170 °C for 3 h. The resulting solution was purified once by centrifugation and redispersion of the pellet in an aqueous solution of HNO_3 (10 mM) followed by dialysis in the same HNO_3 (10 mM) solution for 2 days. Nanorods were then transferred into ethylene glycol (EG) by addition of EG into the aqueous dispersion, and water was removed by distillation using a rotary evaporator. This solution was then put into dialysis for 15 days in EG. The final concentration of the nanorods was 2.8 vol %, which was controlled by the volume of EG added before the solvent exchange.

For the deposition of nanorods-oriented thin films, a homemade blade coater was used to perform a shear-directed assembly.[15] The 15 days-dialyzed nanorod suspension was deposited on a silicon substrate and cut into 6 pieces that were annealed for 1 h at 200, 400, 600, 800, and 1000 °C respectively (ramp of 4 °C/min in a Naberthem furnace), and one remained untreated.

XRD measurements were performed on a Philips X'Pert at $CuK\alpha_{1,2}$ radiation (λ = 1.5409 Å) with a linear detector X'Celerator, and the phase identification was performed with the ICDD PDF-2 database. The calculated cell parameters were obtained by using the MAUD software.[21] High-resolution transmission electron microscopy (HR-TEM) imaging was obtained using a field emission electron gun TEM (JEOL JEM-2010F) operating at 200 kV. Scanning electron microscopy (SEM) imaging was performed on a Hitachi S4800 microscope equipped with a field emission electron gun. Luminescence excitation spectra were measured with a Fluoromax-4 spectrofluorimeter (Horiba Jobin Yvon, 450 W xenon lamp excitation). A femtosecond-pulsed Ti-Sapphire laser combined with a frequency-doubling device was used as excitation source at 394.5 nm for polarized photoluminescence measurements. A multimode optical fiber was used to depolarize the excitation light. The spectra were recorded on an Olympus BX51 microscope combined with a SpectraPro-300i spectrometer from Princeton Instrument, equipped with a LN/CCD-1100-PP camera. On this setup, an achromatic polarizer was used as analyzer for polarization measurements, and a Linkam THMS 600 temperature-controlled stage was used for low temperature measurements. The sample was also excited at 580 nm (direct $^7F_0-^5D_0$ level excitation) by a tunable optical parametric oscillator pumped by a Nd:YAG Q-switched laser (Ekspla NT342B-SH) with 6 ns pulse length, and the luminescence was detected using a Jobin-Yvon HR250 monochromator and a ICCD camera (PI-Max).

RESULTS AND DISCUSSION

The average size of the synthesized nanorods is 150 ± 73 nm in length and 10 ± 2 nm in diameter (Figure 1a, Figure S1). The HR-TEM image (Figure 1b) evidences the monocrystalline nature of the rods and their growth along the [001] direction. The crystallographic *c*-axis is thus parallel to the long axis of the rod. The shear-directed assembly[15] was efficient in preparing a solid film (thickness ~1 μm) of well-aligned nanorods (Figure 1c,d). XRD pattern for the nanorods powder sample (blue line in Figure 1e) matches with the referenced rhabdophane phase of $LaPO_4$ with the hexagonal structure (JCPDS 00-004-0635, black bars in Figure 1e). The experimental lattice parameters are $a = b = 7.01$ Å and $c = 6.52$ Å (space group $P6_222$). The XRD pattern of the rods-aligned film (red line) exhibits missing peaks for $(h,k,l \neq 0)$ which is an apparent texturing effect confirming the in-plane alignment of the nanorods.

The heat treatment at gradually increasing temperatures of the aligned nanorod films shows the different stages of the rhabdophane (hexagonal) to monazite (monoclinic) phase transition, from 200 to 1000 °C. In the series of XRD patterns for each final annealing temperature (T_f) (Figure 2a, whole diagrams are plotted in Figure S2), one can notice the gradual decrease of the hexagonal (100) and (110) peaks up to T_f = 600 °C, a temperature at which the monoclinic (200) peak (at 2θ = 26.88°) begins to appear (yellow arrow). This indicates that the phase transition is triggered at a relatively low temperature, which is consistent with the wide range of the phase transition temperature reported for $LaPO_4$.[16,17,22,23] The calculated coherence lengths L_c of the (110) and (200) planes in the hexagonal phase (Figure S3) are slightly lower than the nanorod diameter observed by SEM (Figure S1). The XRD pattern for T_f = 800 °C corresponds purely to the monoclinic phase (space group $P2_1/c$), with the experimental lattice parameters a = 6.83 Å, b = 7.07 Å, c = 6.50 Å and β = 103.3°, and its peaks remain as wide as the hexagonal peaks for lower T_f. The L_c calculated for the monoclinic (110) and (200) peaks for T_f = 800 °C are 9.5 ± 0.3 nm and 11.6 ± 0.2 nm

DOI: 10.1021/jacs.8b03983
J. Am. Chem. Soc. XXXX, XXX, XXX−XXX

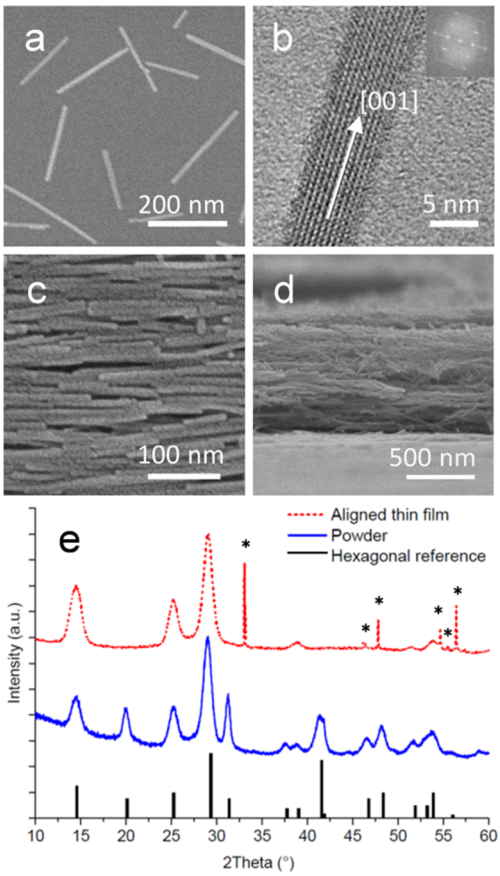

Figure 1. (a) SEM and (b) HR-TEM images of $LaPO_4$:Eu (5%) nanorods. SEM images of (c) the surface and (d) of the cross section of the nanorods-aligned film prepared by a shear-directed assembly. (e) XRD patterns of the aligned nanorod film (red line) and the randomly oriented nanorod powder sample (blue line). The black bars are the reference pattern of the undoped $LaPO_4$ crystals in the rhabdophane phase in the space group $P6_222$ (no. 180, JCPDS 00-004-0635). Asterisks (*) correspond to the peaks for the (400) oriented silicon wafer substrate.

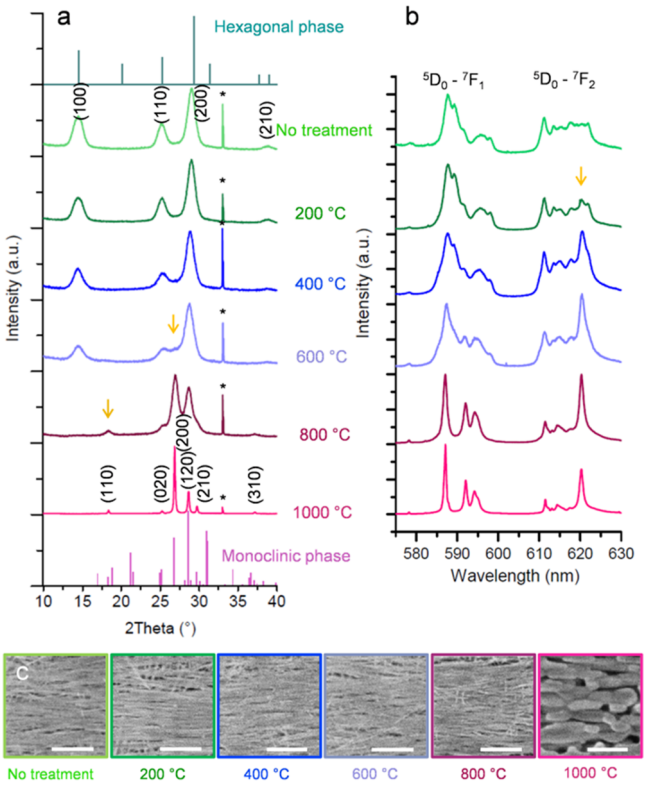

Figure 2. (a) XRD patterns, (b) photoluminescence spectra (λ_{ex} = 394.5 nm, T = 77 K), and (c) SEM images of the aligned $LaPO_4$:Eu (5%) nanorod films for different final annealing temperatures (scale bars 200 nm). Top and bottom patterns in (a) are the reference patterns of the rhabdophane (no. 180 JCPDS 00-004-0635) and the monazite (no. 14 JCPDS 01-084-0600) structures. Asterisks (*) in (a) correspond to the peaks for the (400) oriented silicon wafer substrate.

(Figure S3), which correspond to the diameters of the pristine nanorods. Thus, the phase transition is completed at 600−800 °C, preserving the nanocrystal domain size. A significant decrease of the XRD peak width is observed at T_f = 1000 °C, resulting in $L_c(110)$ = 65 nm (Figure S3). This evidences the sintering process at this high temperature, which is also shown by the large grain size observed in the SEM image (Figure 2c). We note that sintering temperature seems to be distinct from the phase transition temperature. Interestingly, the texturing effect represented by missing peaks for $l \neq 0$ was perfectly preserved during the phase transition and sintering processes. This indicates that the initial alignment of the crystallographic *c*-axis (parallel to rod axis) was maintained as similarly observed for a powder sample.[22] Such a persistent *c*-axis alignment was the key to the consistent analysis of the polarized luminescence of the $LaPO_4$:Eu polymorphs which is discussed below.

Eu^{3+} is well-known to be a convenient probe to determine crystalline structure[24,25] and site symmetries[26] or to detect distortions in crystals.[8,27] We utilized this to continuously track the phase transition of the $LaPO_4$:Eu nanocrystals. When Eu^{3+} dopants are excited at 394.5 nm, corresponding to the $^7F_0$−$^5L_6$ transition (the excitation spectrum is shown in Figure S4), they first relax by nonradiative transitions to the $^5D_0$ singlet, then by radiative transition to the ^7F_J multiplet yielding the spiky spectrum which is a typical characteristic of Eu^{3+} luminescence[10] (Figure S5). We focused on the two most intense bands for $^5D_0$−$^7F_1$ and $^5D_0$−$^7F_2$ transitions that respectively have a magnetic dipole nature and an electric dipole nature.[10] In the series of emission spectra for different T_f (Figure 2b), the variation of the spectral line shape is clearly visible, especially for the $^5D_0$−$^7F_2$ band which is known to be "hypersensitive" to the environment of the emitter ion.[10] The peak at 620 nm, which is the most intense $^5D_0$−$^7F_2$ sublevel for the monoclinic phase, begins to appear already at T_f = 200 °C (yellow arrow) and reaches a significant intensity at T_f = 400 °C, while in the XRD patterns the monoclinic peaks are difficult to identify until T_f = 600 °C. Therefore, the early phase transition occurring at low temperature in a minor volume becomes detectable through the Eu^{3+} spectroscopy. This high sensitivity is attributed to the high emission efficiency of the monoclinic phase[28,29] compared to the hexagonal phase. An increase by a factor of 8 was observed by comparing the emission intensity of the initial rhabdophane film and the 1000 °C treated monazite one (Figure S6). At 800 and 1000 °C (Figure 2b), the contribution of the hexagonal phase has vanished, and the luminescence spectra display the typical emission line shape of the monoclinic phase.[30] The progressive evolution of the spectra thus suggests that the phase transition of these nanocrystals occurs continuously

DOI: 10.1021/jacs.8b03983
J. Am. Chem. Soc. XXXX, XXX, XXX−XXX

between 200 and 800 °C probably starting at the nanorod surface or on defects.

In a crystalline matrix, the crystal field influences the emission of lanthanide dopants. The Stark effect splits degenerate transitions into multiple sublevels whose number and wavelengths are determined by the site symmetry of the emitter ion.[31] La^{3+} sites of $LaPO_4$ possess D_2 and C_1 symmetries in rhabdophane and monazite phases, respectively[32] (Figure 3a,b). The substitutional Eu^{3+} should possess

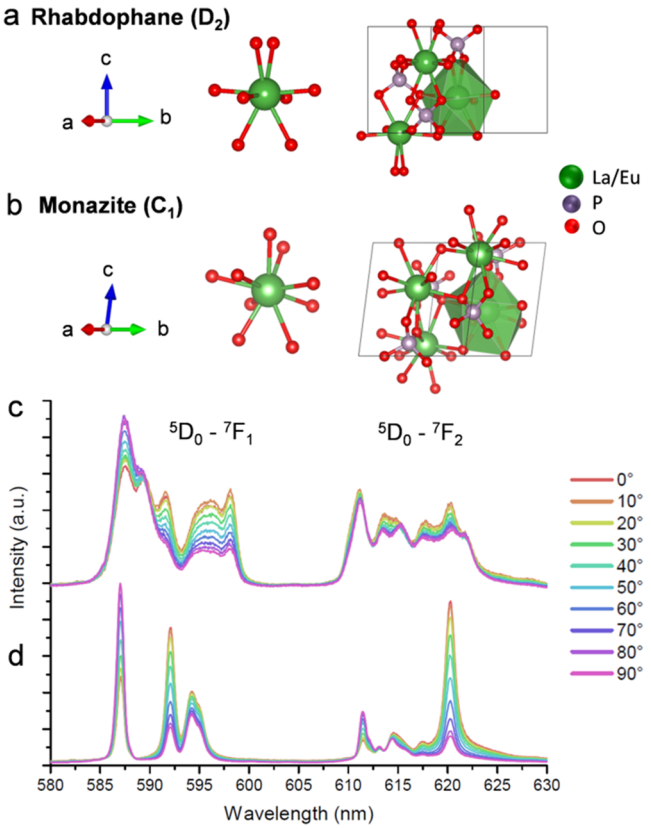

Figure 3. (a,b) Illustration of the crystallographic structures and the site symmetries of (a) rhabdophane (hexagonal system, SG $P6_222$, symmetry site D_2) and (b) monazite (monoclinic system, SG $P2_1/c$, site symmetry C_1) phases of $LaPO_4$. (c,d) Polarized emission spectra of the aligned nanorod films of $LaPO_4$:Eu (5%) in (c) rhabdophane phase without annealing and (d) monazite phase annealed at T_f = 1000 °C (λ_{ex} = 394.5 nm, 77 K). The 0° angle corresponds to the polarization parallel to the rod alignment (π configuration), and the 90° corresponds to the perpendicular direction (σ configuration).

the same site symmetries. The group theory predicts triplets for the $^5D_0$–$^7F_1$ transition in both D_2 and C_1 symmetries, while a triplet and a quintet are expected for the $^5D_0$–$^7F_2$ in the D_2 and C_1 symmetries, respectively.[33] However, a larger number of peaks are obviously recognizable on the experimental spectra, especially in the case of the rhabdophane phase (Figure 2b). This spectral feature was found unchanged under direct excitation of the $^5D_0$ level at 580 nm (Figure S7), eliminating the possibility of the transitions from $^5D_{J>0}$ levels.[34] We thus attribute the extra number of peaks to the structural defects, in volume and/or surface sites,[35] which may be prevalent in the rhabdophane phase due to the mild synthesis condition in solution compared to the bulk material.[34] Such defects can easily cause symmetry breaking[7] and duplication of the sites,[36] increasing the number of peaks compared to the perfect crystal structure. The number of peaks did not change when the Eu^{3+} doping concentration was changed from 0.1% to 20% (see Figure S8), supporting that the population of neighboring Eu^{3+} ions is not the main reason. However, it is still possible that some Eu^{3+} dopants have clustered or segregated inhomogeneously during the synthesis causing the transition sublevel energies distinct from those of isolated Eu^{3+} ions.[37] In addition, a lattice deformation caused by the water molecules in the rhabdophane phase[38] could also have increased the number of peaks. Further experiments are required to investigate the precise crystallographic structure of our rhabdophane phase. In the case of monazite phase, the sharp and less complicated spectrum denotes elimination of some defects during annealing. The shoulder peaks that are still present (e.g., at 588 and 595 nm) can be attributed to the defects possibly inherent to the doping sites due to the ionic radii of Eu^{3+} (106.6 pm in a 8 coordination; 112.0 pm in a 9 coordination) smaller than those of La^{3+} (116.0 pm with 8 coordinates, 121.6 pm with 9 coordinates).[39] The contribution of the surface sites in the monoclinic phase seems to be minor since the shoulder peaks persist during the grain growth led by the sintering process (T_f = 1000 °C).

A remarkable feature of the lanthanide luminescence is that each of the narrow sublevel transitions can hold independently a principal polarization configuration. This polarization is determined by the site symmetry of the emitting lanthanide ion and is either perpendicular (σ) or parallel (π) to the preferential symmetry axis of the crystal when this preferential axis exists. This property was previously used for the precise assignment of the numerous transition levels in europium complexes[24,40−42] or europium-doped single crystals.[6−8,43] This polarized luminescence leads to a dramatic line shape variation of the emission spectrum when observing a crystallite through a rotating polarizer.[44] We observed such anisotropic emission spectra depending on the gradual polarizer angles from the aligned films of the two $LaPO_4$:Eu nanorod polymorphs (Figure 3c,d) by virtue of the conserved c-axis orientation during the phase transition, as discussed earlier. Measurements performed on randomly oriented $LaPO_4$:Eu nanorod powders did not show polarization (Figure S9).

Although the theory[45−47] assigns a sublevel to either purely σ or purely π polarization when the emitter ions are in D_2 symmetry sites (Table S1) and one of the C_2 symmetry axis being parallel to the c-axis of the host crystal (Figure 3a), in the real case, each peak displays a partial degree of polarization, DOP = $(I_{\|} - I_{\perp})/(I_{\|} + I_{\perp})$, due to the high sensitivity of the crystal field to even slight distortions of the site symmetry.[7,8] The calculated DOP thus is equal to 1 and −1 if the polarization is purely π and σ, respectively. In the rhabdophane phase, the $^5D_0$–$^7F_1$ sublevels are visibly polarized (Figure 3c), which allows us to assign their principal configurations (Table 1) by performing a peak deconvolution (Figure S10) and comparing with the expected polarizations (Table S1). However, the $^5D_0$–$^7F_2$ sublevels are all very weakly polarized and difficult to analyze. In the monazite phase, by contrast, the polarization is much more prominent in both $^5D_0$–$^7F_1$ and $^5D_0$–$^7F_2$ transitions (Figure 3d). Each sublevel peak is sharp and well-separated, allowing a precise measurement of the DOP (Table 1). Especially, the most intense $^5D_0$–$^7F_2$ sublevel at 620 nm is extremely highly π-polarized (DOP = 69%). For C_1 site symmetry, which is the lowest symmetry, the group theory does not assign a polarization preferentially to one particular axis of the crystal (Table S1). Nevertheless, σ and π

DOI: 10.1021/jacs.8b03983
J. Am. Chem. Soc. XXXX, XXX, XXX−XXX

Table 1. Polarization of the Photoluminescence Peaks Observed from the Aligned $LaPO_4$:Eu Nanorods (λ_{ex} = 394.5 nm, 77 K)[a]

crystalline phase	transition	wavelength (nm)	polarization	initial and final states	DOP (%)
rhabdophane (D_2)	$^5D_0 - {}^7F_1$	587.4	σ	A → B1	−16[b]
		589.7	π	A → B2 or B3	+7.7[b]
		591.6	π		+46[b]
		596.0	π	A → B3 or B2	+39
		598.1			+43
monazite (C_1 close C_s)	$^5D_0 - {}^7F_1$	587.1	σ	A′ → A′	−35
		592.0	π	A′ → A″	+56
		594.2	π	A′ → A″	+19
		595.0			+21
	$^5D_0 - {}^7F_2$	611.5	σ	A′ → A′	−35
		612.2			−21
		613.2	σ	A′ → A′	−4.9
		614.5	π	A′ → A″	+13
		615.7			+17
		617.4	π	A′ → A″	+37
		620.2	π	A′ → A″	+69

[a]The assignments correspond to the configurations of the D_2 and C_s symmetries, respectively, for the rhabdophane and monazite phases. [b]Corresponds to the degree of polarizations (DOPs) calculated from deconvoluted spectra (Figure S10).

polarizations can be observed with C_1 sites[48] as the crystal symmetry induces a periodicity of C_1 sites that may produce polarizations globally oriented to the crystal axes. Local deformation of the C_1 symmetry could also be the origins of the observed high DOP.[7] In the monazite structure, although the Eu^{3+} site is assigned to be in the C_1 symmetry, it differs only slightly from the higher C_s symmetry (Figure S11) which should produce well-defined σ and π polarizations. Indeed, the polarizations measured for the monoclinic phase (Table 1) is similar to the group theory assignments for the C_s symmetry (Table S1). In both phases, some adjacent peaks display almost the same DOPs (e.g., 595−598 nm in rhabdophane, 594−595 nm in monazite). This fact also supports the above-stated hypothesis of distorted or clustered Eu^{3+} sites contributing to the extra peaks, because their symmetry nature would be close to that of the original sites.

CONCLUSIONS

To conclude, observing the Eu^{3+} dopant luminescence is shown to be more sensitive to the phase transition of the $LaPO_4$:Eu nanocrystals than the X-ray diffraction analysis with a laboratory diffractometer. This suggests that the lanthanide dopant luminescence is a versatile and complementary indicator for the structural evolution of various phase changing materials. Such a spectroscopic analysis has an advantage of easiness for adapting to different experimental setups (e.g., optical microscopes) that are often not compatible with X-ray instruments. Especially, it is promising for the in situ measurement of materials in small amounts down to the single nanoparticle level.

The distinct polarization features of the $LaPO_4$:Eu polymorphs highlight the strong influence of the crystal structure and defects on the dipolar nature of the Eu^{3+} sublevel transitions. This is consistent with the site symmetry modification from D_2 to C_1 being close to distorted C_s during the phase transition. Indeed, the high DOP obtained in both the $^5D_0 - {}^7F_1$ (magnetic dipolar transition) and $^5D_0 - {}^7F_2$ (electric dipolar transition) levels for the monazite phase enables precise determination of the crystal orientation in three dimensions. The peak ratiometry in each level provides one angular information, thus the two levels can be simultaneously treated to calculate the two spherical angles defining the crystal (rod) axis.[44] This provides a novel functionality of sensing the orientation and rotation which is applicable to bioimaging or microfluidics.[44] For this purpose, the direct synthesis of colloidal monazite nanorods would be valuable and is a subject of our ongoing investigations.

ASSOCIATED CONTENT

Supporting Information

The Supporting Information is available free of charge on the ACS Publications website at DOI: 10.1021/jacs.8b03983.

DOI: 10.1021/jacs.8b03983
J. Am. Chem. Soc. XXXX, XXX, XXX−XXX

Nanoparticle size analysis, XRD patterns for the full 2θ range, coherence length (L_c) analysis, excitation spectrum and full emission spectrum of $LaPO_4$:Eu, comparison of the emission intensities in the different crystal phases and during the heat treatment, emission spectrum for the direct $^7F_0$-$^5D_0$ excitation, emission spectra for different Eu^{3+} doping concentrations in $LaPO_4$:Eu, table for the polarization assignments by the selection rules, polarized spectra of powders, peak deconvolution study of the polarized emission spectrum, schematic of the C_s symmetry site (PDF)

AUTHOR INFORMATION

Corresponding Authors

*thierry.gacoin@polytechnique.edu
*jong-wook.kim@polytechnique.edu

ORCID

Thierry Gacoin: 0000-0001-6774-3181

Funding

Part of this work was supported by the French National Research Agency (ANR) in the frame of the SpecTra project (ANR-16-CE24-0014).

Notes

The authors declare no competing financial interest.

ACKNOWLEDGMENTS

The authors acknowledge Eric Larquet for the TEM.

REFERENCES

(1) Grell, M.; Bradley, D. D. C. *Adv. Mater.* **1999**, *11*, 895.
(2) Hu, J.; Li, L.-s.; Yang, W.; Manna, L.; Wang, L.-w.; Alivisatos, A. P. *Science* **2001**, *292*, 2060.
(3) Wang, J.; Gudiksen, M. S.; Duan, X.; Cui, Y.; Lieber, C. M. *Science* **2001**, *293*, 1455.
(4) Breen, C. A.; Deng, T.; Breiner, T.; Thomas, E. L.; Swager, T. M. *J. Am. Chem. Soc.* **2003**, *125*, 9942.
(5) Hsu, N. E.; Hung, W. K.; Chen, Y. F. *J. Appl. Phys.* **2004**, *96*, 4671.
(6) Brecher, C.; Samelson, H.; Lempicki, A.; Riley, R.; Peters, T. *Phys. Rev.* **1967**, *155*, 178.
(7) Brecher, C. *J. Chem. Phys.* **1974**, *61*, 2297.
(8) Moret, E.; Nicolo, F.; Bunzli, J. C. G.; Chapuis, G. *J. Less-Common Met.* **1991**, *171*, 273.
(9) Kan, S.; Mokari, T.; Rothenberg, E.; Banin, U. *Nat. Mater.* **2003**, *2*, 155.
(10) Binnemans, K. *Coord. Chem. Rev.* **2015**, *295*, 1.
(11) Lisiecki, R.; Solarz, P.; Dominiak-Dzik, G.; Ryba-Romanowski, W.; Sobczyk, M.; Cerny, P.; Sulc, J.; Jelinkova, H.; Urata, Y.; Higuchi, M. *Phys. Rev. B: Condens. Matter Mater. Phys.* **2006**, *74*, 035103.
(12) Liu, Q.; Sun, Y.; Yang, T. S.; Feng, W.; Li, C. G.; Li, F. Y. *J. Am. Chem. Soc.* **2011**, *133*, 17122.
(13) Dong, H.; Du, S. R.; Zheng, X. Y.; Lyu, G. M.; Sun, L. D.; Li, L. D.; Zhang, P. Z.; Zhang, C.; Yan, C. H. *Chem. Rev.* **2015**, *115*, 10725.
(14) Kim, J.; de la Cotte, A.; Deloncle, R.; Archambeau, S.; Biver, C.; Cano, J.-P.; Lahlil, K.; Boilot, J.-P.; Grelet, E.; Gacoin, T. *Adv. Funct. Mater.* **2012**, *22*, 4949.
(15) Kim, J.; Peretti, J.; Lahlil, K.; Boilot, J. P.; Gacoin, T. *Adv. Mater.* **2013**, *25*, 3295.
(16) Glorieux, B.; Matecki, M.; Fayon, F.; Coutures, J. P.; Palau, S.; Douy, A.; Peraudeau, G. *J. Nucl. Mater.* **2004**, *326*, 156.
(17) Colomer, M. T.; Mosa, J. *Ceram. Int.* **2015**, *41*, 8080.
(18) Zhou, J.; Chen, G.; Wu, E.; Bi, G.; Wu, B.; Teng, Y.; Zhou, S.; Qiu, J. *Nano Lett.* **2013**, *13*, 2241.
(19) Rodriguez-Sevilla, P.; Labrador-Paez, L.; Wawrzynczyk, D.; Nyk, M.; Samoc, M.; Kar, A. K.; Mackenzie, M. D.; Paterson, L.; Jaque, D.; Haro-Gonzalez, P. *Nanoscale* **2016**, *8*, 300.
(20) Chen, P.; Song, M.; Wu, E.; Wu, B.; Zhou, J.; Zeng, H.; Liu, X.; Qiu, J. *Nanoscale* **2015**, *7*, 6462.
(21) Lutterotti, L. M.; Matthies, S.; Wenk, H. -R. MAUD (Material Analysis Using Diffraction): a user friendly Java program for Rietveld Texture Analysis and more. Proceedings of the *Twelfth International Conference on Textures of Materials (ICOTOM-12)*, Montreal, Canada, August 9-13, 1999; NRC Research Press: Ottawa, Canada, 1999, Vol. *2*, pp 1599−1604.
(22) Zheng, Q.; Wang, X.; Tian, J.; Kang, R.; Yin, Y. *Mater. Chem. Phys.* **2010**, *122*, 49.
(23) Li, J.; Xu, X.; Fan, Y.; Li, Y.; Hu, L.; Tang, C. *Mater. Chem. Phys.* **2010**, *124*, 1172.
(24) Durham, D. A.; Frost, G. H.; Hart, F. A. *J. Inorg. Nucl. Chem.* **1969**, *31*, 833.
(25) Seminara, A.; Musumeci, A. *Inorg. Chim. Acta* **1984**, *95*, 291.
(26) Gupta, S. K.; Bhide, M. K.; Godbole, S. V.; Natarajan, V.; Ballato, J. *J. Am. Ceram. Soc.* **2014**, *97*, 3694.
(27) Tu, D. T.; Liu, Y. S.; Zhu, H. M.; Li, R. F.; Liu, L. Q.; Chen, X. Y. *Angew. Chem., Int. Ed.* **2013**, *52*, 1128.
(28) Ferhi, M.; Horchani-Naifer, K.; Ferid, M. *J. Lumin.* **2008**, *128*, 1777.
(29) Ghosh, P.; Patra, A. *J. Nanosci. Nanotechnol.* **2008**, *8*, 3458.
(30) DexpertGhys, J.; Mauricot, R.; Faucher, M. D. *J. Lumin.* **1996**, *69*, 203.
(31) Hänninen, P.; Härmä, H. *Lanthanide Luminescence: Photophysical, Analytical and Biological Aspects*; Springer-Verlag: Berlin, 2011.
(32) Henry, N. F.; Lonsdale, K. *International Tables for X-Ray Crystallograhy*, 3rd ed.; Kynoth Press: Birmingham, UK, 1969; Vol. *I*, Symmetry Groups.
(33) Tanner, P. A. *Chem. Soc. Rev.* **2013**, *42*, 5090.
(34) Fang, Y. P.; Xu, A. W.; Song, R. Q.; Zhang, H. X.; You, L. P.; Yu, J. C.; Liu, H. Q. *J. Am. Chem. Soc.* **2003**, *125*, 16025.
(35) Lehmann, O.; Kömpe, K.; Haase, M. *J. Am. Chem. Soc.* **2004**, *126*, 14935.
(36) Holliday, K. S.; Babelot, C.; Walther, C.; Neumeier, S.; Bosbach, D.; Stumpf, T. *Radiochim. Acta* **2012**, *100*, 189.
(37) Lochhead, M. J.; Bray, K. L. *Chem. Mater.* **1995**, *7*, 572.
(38) Mesbah, A.; Clavier, N.; Elkaim, E.; Gausse, C.; Kacem, I. B.; Szenknect, S.; Dacheux, N. *Cryst. Growth Des.* **2014**, *14*, 5090.
(39) Shannon, R. D. *Acta Crystallogr., Sect. A: Cryst. Phys., Diffr., Theor. Gen. Crystallogr.* **1976**, *32*, 751.
(40) Blanc, J.; Ross, D. L. *J. Chem. Phys.* **1965**, *43*, 1286.
(41) Lagerwey, A. A. F.; Blasse, G. *Chem. Phys. Lett.* **1975**, *31*, 27.
(42) Peacock, R. D. *Chem. Phys. Lett.* **1975**, *35*, 420.
(43) Gorllerwalrand, C.; Hendrickx, I.; Fluyt, L.; Bunzli, J. C. G.; Moret, E. *Chem. Phys. Lett.* **1990**, *170*, 223.
(44) Kim, J.; Michelin, S.; Hilbers, M.; Martinelli, L.; Chaudan, E.; Amselem, G.; Fradet, E.; Boilot, J. P.; Brouwer, A. M.; Baroud, C. N.; Peretti, J.; Gacoin, T. *Nat. Nanotechnol.* **2017**, *12*, 1015.
(45) Görller-Walrand, C.; Binnemans, K. In *Handbook on the Physics and Chemistry of Rare Earths*; Elsevier: Amsterdam, 1996; Vol *23*, p 121.
(46) Powell, R. C. *Symmetry, Group Theory, and the Physical Properties of Crystals*; Springer: Heidelberg, 2010.
(47) Atkins, P. W.; Child, M. S.; Phillips, C. S. G. *Tables for Group Theory*; Oxford Higher Education: Oxford, 1970.
(48) Konz, F.; Sun, Y.; Thiel, C. W.; Cone, R. L.; Equall, R. W.; Hutcheson, R. L.; Macfarlane, R. M. *Phys. Rev. B: Condens. Matter Mater. Phys.* **2003**, *68*, 085109.

DOI: 10.1021/jacs.8b03983
J. Am. Chem. Soc. XXXX, XXX, XXX−XXX